Available online at www.sciencedirect.com
SCIENCE DIRECT®
Microporous and Mesoporous Materials 61 (2003) 3–24
MICROPOROUS AND MESOPOROUS MATERIALS
www.elsevier.com/locate/micromeso

Review

HEU-type zeolites modified by transition elements and lead

Ath. Godelitsas [a,*], Th. Armbruster [b,1]

[a] Westfälische Wilhelms-Universität Münster, Institut für Mineralogie, Corrensstraße 24, Münster D-48149, Germany
[b] Universität Bern, Laboratorium für chemische und mineralogische Kristallographie, Freiestrasse 3, Bern CH-3012, Switzerland

Received 22 July 2002; received in revised form 10 February 2003; accepted 11 February 2003

Abstract

Research on pure samples of **HEU**-type zeolites modified by d- and f-block transition elements and Pb is reviewed. The interest on such modified **HEU**-type zeolites mainly arises from their use in pollution abatement, and for their potential catalytic properties. In addition, new composite materials composed of transition-metal loaded crystals with organic complexes stabilised on the zeolite substrate are gaining importance for versatile applications.

If sorption is governed by ion-exchange, the structural distribution of the transition elements can be determined by single-crystal XRD. In more complicated cases, where an intense metal accumulation is observed on the surface of the crystals, the structural characteristics can only be defined using a combination of microscopic, spectroscopic, and thermal techniques.

Detailed crystal-structure information is available for **HEU**-type crystals completely cation exchanged by Ag^{+}, Pb^{2+}, Cd^{2+}, Mn^{2+}, and Cu^{2+}. Cd^{2+}, Cu^{2+} and Mn^{2+} mainly occupy two extra-framework sites: one in the centre of the ten-membered ring, octahedrally coordinated by six H_2O molecules, and one in the eight-membered ring, coordinated to framework oxygen and additional H_2O. Ag^{+} and Pb^{2+} do not occupy the centre of the ten-membered ring but are shifted towards the framework walls.

Complementary microscopic, spectroscopic, and thermal data (e.g. SEM-EDS, IR, EPR, NMR, EXAFS, XPS, RBS, DTA, TPD) on heulandite and clinoptilolite interacted with Co, Ni, Cu, Pd and Hg indicated non-homoionic and non-stoichiometric metal-loading. Excessive accumulation on the crystal surface, due to adsorption and surface precipitation phenomena, was commonly observed.

Only very low incorporation of trivalent ions of lanthanides/rare-earth elements into the heulandite channel system was experimentally achieved. Th^{4+}- and UO_2^{2+}-ions interact significantly with heulandite but the metal sorption is mainly attributed to adsorption and surface precipitation processes.

Keywords: Microporous materials; Aluminosilicates; Zeolites; Heulandite; Clinoptilolite; Transition elements; Ion-exchange; Sorption; Adsorption; Surface precipitation

* Corresponding author. Tel.: +49-251-8333502; fax: +49-251-8338397.
E-mail addresses: athgod@nwz.uni-muenster.de (Ath. Godelitsas), thomas.armbruster@krist.unibe.ch (Th. Armbruster).
[1] Tel.: +41-31-6314266; fax: +41-31-6313996.

1387-1811/03/$ - see front matter
doi:10.1016/S1387-1811(03)00352-4

Contents

1. Introduction

1.1. Definition of heulandite and clinoptilolite

In the past heulandite and clinoptilolite, with a common **HEU** framework topology, were distinguished based on their behaviour upon heat treatment and on chemical grounds [1–9]. However, according to the Zeolite Subcommittee of the Commission on New Minerals and Mineral Names of the International Mineralogical Association (IMA) [10] heulandite is defined as the zeolite mineral series having the distinctive framework topology of heulandite and the ratio $Si/Al < 4$, while clinoptilolite is defined as the series with the same framework topology and $Si/Al > 4$. The committee [10] and also Bish and Boak [11] noticed that although thermal stability is useful as an aid to identification, it is not appropriate as the basis for definition. Heulandite and clinoptilolite cannot be distinguished solely on the basis of XRD because the unit-cell parameters are sensitive to changes in water content and extra-framework cation composition. Thus a chemical characterisation becomes essential. In addition, Passaglia and Sheppard [12] argued that although many zeolite samples have been described as heulandite or clinoptilolite on the basis of chemical parameters and/or thermal behaviour, several definitions are based only on the occurrence; the name 'heulandite' is used for samples in vugs of igneous rocks while 'clinoptilolite' for samples in sedimentary (mostly commercialised) rocks. They therefore described in their review heulandite and clinoptilolite without further distinction.

In order to surpass the above mineralogical–geological puzzle, the Structure Commission of the International Zeolite Association (IZA) focused

on the common structural characteristics of the two species and gave a simple technical answer by using the single framework code **HEU** [13] for both natural heulandite and clinoptilolite as well as for relevant synthetic zeolites with the same topology including LZ-219 and CIT-3 e.g. [14–17].

The naturally occurring **HEU**-type zeolites are the most abundant minerals on earth, exhibiting a zeolite structure. They are mostly found in specific types of sedimentary rocks (tuffs) in the form of small crystals (0.1–100 μm) associated with clays and other silicate and aluminosilicate phases of similar density. However, even centimeter-scale single crystals can grow in cavities of igneous rocks from natural hydrothermal solutions. Tuffs containing crystals of **HEU**-type zeolites (zeoliferous rocks) form large deposits in many areas, such as the USA, Japan, the former Soviet Union, Hungary, Bulgaria, Australia, China, Italy, Greece, and Mexico, and provide low-cost industrial minerals with several commercial applications e.g. [18–25]. The synthetic zeolite species such as LZ-219 and CIT-3, are all more expensive microporous solids, as yet without extensive practical applications.

1.2. The HEU-type structure

The crystal structure of the **HEU**-type zeolites [13,25–29] is characterised by a three-dimensional aluminosilicate framework consisting fundamentally of secondary building units (SBUs) of the 4–4–1 type, formed by TO_4 (T = Si, Al) tetrahedral primary building units (PBUs). Chain-like structural sub-units (SSUs) of the *heulandite* type originate from these SBUs, and are further combined through 4.5^2-type SSUs to form structural "sheets" parallel to the (0 1 0). For this spatial arrangement of SSUs, the framework contains narrow four- and five-membered rings, as well as broad eight- and ten-membered rings constituting intraframework micropores (channels) capable of hosting extra-framework/exchangeable cations (e.g. Na^+, K^+, Ca^{2+}) in association with mobile H_2O molecules. The crystals of **HEU**-type zeolites (Fig. 1) accommodate two different systems of micropores interconnected within the lattice, the first developed along the *c*-axis with both eight- and ten-membered rings forming A- and B-type channels (3.3×4.6 and 3.0×7.6 Å, respectively), and the second developed along the [1 0 2] and the *a*-axis with eight-membered rings forming C-type channels (2.6×4.7 Å).

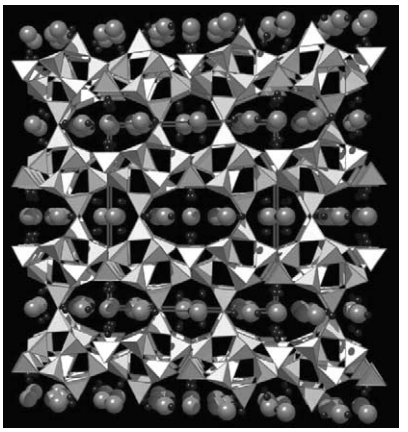

Fig. 1. Polyhedral model of the **HEU**-type framework projected parallel to the *c*-axis. Large light grey spheres represent extra-framework cations in the ten-membered A and eight-membered B channels. Small dark grey spheres are H_2O molecules. In addition, unit cell outlines are displayed.

1.3. Sorption properties of HEU-type structures

The relatively 'open' structure of **HEU**-type zeolites, with a total pore volume (TPV) of 35%, enhances the sorption properties of these microporous solids, especially towards gaseous molecules such as dinitrogen, water, carbon monoxide, ammonia, methanol, methane and pyridine, which are small enough to enter the channels. The TPV of zeolite crystals is correlated with the crystallographic arrangement of the aluminosilicate framework, and particularly with the framework density (FD), which is 17.1 $T_{sites}/1000$ Å^3 for the **HEU**-type structure. However, the chemical composition of the framework (the Si/Al ratio, in the range 3–5) modulates the ion-exchange properties of the zeolites expressed as cation-exchange capacity (CEC, which can theoretically reach 330 meq/100 g). The rather low Si/Al ratio and the consequently increased CEC render HEU-type zeolites advantageous for binding dissolved cations from aqueous solutions. Of particular interest is the interaction of **HEU**-type zeolites with

metallic cations (mostly heavy metals) which are sorbed by the zeolite and immobilised in the crystals, modifying the initial **HEU**-type structure. This is crucial for environmental technology (for example, decontamination of wastewaters) and for certain industrial applications. The dissolved metallic cations interact with the **HEU**-type zeolite crystals, and they are subsequently removed from the solution, through different sorption mechanisms including principally the so-called 'ion-exchange'. A typical 'ion-exchange' mechanism is supposed to be a reversible chemical reaction wherein an ion from solution is exchanged for a similarly charged ion which is initially bonded to a solid behaving as 'ion-exchanger'. In the case of the zeolites ion-exchange is practically a cation-exchange reaction which, for a binary process involving A^{Z_a} and B^{Z_b} dissolved cations, can simplified expressed as $z_b A^{Z_a} + z_a \bar{B}^{Z_b} \rightleftharpoons z_b \bar{A}^{Z_a} + z_a B^{Z_b}$ where $z_{a,b}$ represent the valence of the respective cations and $\bar{B}$ and $\bar{A}$ are exchangeable cations in the solid (e.g. $2Na^+ + \overline{Ca}^{2+} \rightleftharpoons 2\overline{Na}^{+} + Ca^{2+}$). The binary exchange may be described by an ion-exchange isotherm which fundamentally defines the equilibrium at a specified temperature and solution normality, and further reveals on the basis of its shape the preference or 'selectivity' of the zeolite for ion A^{Z_a} relative to ion B^{Z_b} in terms of a selectivity coefficient e.g. [21,30]. The sorption of metallic cations from aqueous solutions by **HEU**-type zeolite crystals via ion-exchange seems to be affected by a combination of factors corresponding to the physicochemical characteristics of both the solution and the solid. First of all, ion-exchange depends on the temperature, the solution pH, the concentration, and especially on the hydrated ionic radii of the dissolved ions as correlated to the zeolitic channels. It should be noticed that the radius of a fully hydrated ion is proportional to the ionic charge (valence) but not proportional to the ionic radius without H_2O shell. For example, Cs^+ (ionic radius 1.69 Å and hydrated radius 3.29 Å) is exchanged more easily than Li^+ (ionic radius 0.60 Å but hydrated radius 3.82 Å) or even than Be^{2+} (ionic radius 0.31 Å and hydrated radius 4.59 Å) e.g. [31,32]. On the other hand, the elevated temperature normally enhances the ion-exchange reactions while the pH is also critical (specifically in the case of acidic solutions) because the small H^+ cations are very mobile and reactive over any other metallic cations. Therefore, the most optimum conditions for successful metal-loading should be related to exchange of cations of low valence and large ionic radius (small hydrated radius) by using increased temperature, and rather high pH in order to minimise the effect of H^+ cations. Others factors which should be taken into account concern the solid/liquid ratio, the zeolite particles-size (high specific surface area favours the ion-exchange) and of course the treatment time which must be likely long and combined with renewals of the solution (step-by-step ion-exchange). In fact, the above statements are strictly valuable mostly for the alkali and alkaline earth element cations which are practically stable in aqueous solutions with respect to further hydrolysis reactions. As a result, the corresponding partially or even fully exchanged (homoionic) forms of **HEU**-type zeolites can be achieved by regulating the aforementioned factors. In contrast, the situation is more complicated for many of the transition element cations which are unstable and preferably hydrolysed e.g. [33]. In most of the cases the hydrolysis is unavoidable because the pH increases rapidly due to simultaneous H^+ sorption, or because of the elevated temperature chosen for sufficient metal-loading. Therefore, the uptake of transition elements such as Co, Ni, Hg, Th and U, strongly depends on their aqueous chemistry and particularly on hydrolysis reactions yielding a variety of soluble and insoluble hydrolysis products (ionic and even neutral species) which interact with the microporous zeolitic solid. As a consequence the sorption mechanisms do not comprise ion-exchange (which is a kind of bulk sorption, i.e. *ab*sorption into the channels of the tetrahedral framework), but also *ad*sorption (specific and/or non-specific regarding inner-sphere and/or outer-sphere surface complexation) and surface precipitation/co-precipitation e.g. [34,35]. The corresponding metal-loaded **HEU**-type crystals (metal-forms) are usually non-homoionic because major extra-framework cation sites are inaccessible to bulky aqueous complexes/hydrolysis products. In addition, these metal-forms can be non-stoichiometric with irregular metal distribu-

tion throughout the structure, or even real composite materials containing absorbed (ion-exchanged) metal cations in the micropores as well as metal ions and distinct metal phases (e.g. hydroxides) supported onto the surface. It should be emphasised that since the metal sorption mechanisms are related to surface chemical processes, the surface morphology (concerning cleavage macrosteps, and small fractures/cracks which are actually mesopores and macropores), and the surface microtopography (concerning microsteps, kinks, and terrace vacancies constituting possible additional micropores) play also an important role.

1.4. Modified HEU-type zeolites

According to the literature, the modification of **HEU**-type zeolites with typical transition elements and lead (heavy metals) is commonly achieved by treatment in aqueous solutions of corresponding salts (chlorides, nitrates, acetates) using the fully Na^+-exchanged (homoionic) form as precursor phase. If the sorption is governed by ion-exchange (with subsequent replacement of Na^+ cations in the channels), the structural distribution of the sorbed elements and their influence on the tetrahedral framework structure can be determined by means of single-crystal XRD. In more complicated cases, where an intense metal accumulation is observed on the surface of the crystals, the structural characteristics can only be defined using a combination of spectroscopic, thermal, and other techniques. In the development of transition metal based catalysts, precise characterisation of the chemically modified (metal-loaded) zeolite and thorough investigation of the chemical properties of the solid, with particular emphasis on the definition of potential structural Lewis- and/or Brønsted-type active sites, are also essential.

In general, three types of starting materials could be used to characterise **HEU**-type zeolites modified with transition elements and lead: (1) natural 'heulandite' crystals crushed and sieved to the appropriate size, (2) synthetic 'clinoptilolite' powders, and (3) 'clinoptilolite'-containing tuffs (with additional glass, clays, feldspars, quartz, etc.). However, to distinguish heavy metal surface adsorption or precipitation from incorporation into the structural voids, only natural 'heulandite' and pure synthetic phases are appropriate because in these materials the unpredictable effect of admixtures can be excluded. Studies performed on 'clinoptilolite' bearing tuffs are for this reason not considered in the review.

2. Metal-forms (MnHEU, CuHEU, AgHEU, CdHEU, REEHEU, PbHEU) studied by single-crystal XRD

2.1. General aspects of single-crystal X-ray structure refinements of HEU-type zeolites

If cation-exchanged single-crystals (≈0.1 mm in minimum dimension) are available standard X-ray structure solution-refinement has the big advantage that this method is 'blind' for surface sorption effects (*ad*sorption) and resolves only exchanged cations in the interior of the crystal. The accuracy of the refined occupancy of a specific extra-framework site strongly depends on the number of electrons of the chemical species and its either static or dynamic translational disorder. With synchrotron X-radiation even significantly smaller crystals may be investigated. One way to test the quality of the refinement is a comparison of the extra-framework cation-content with a bulk-analytical technique, e.g. electron microprobe-analysis, of a corresponding crystal. If the structural model is approximately correct, a similar number of extra-framework cations should be analysed by chemical and structural investigation. One puzzling example exists in the literature which does not fulfil the above criterion [36]: two natural heulandite samples were exchanged with 1 M $AgNO_3$ solution. One sample was treated at 160 °C (5 days) and the other at 210 °C (12 days). Subsequent electron microprobe analyses yielded for both the composition $Ag_{7.3}\,[Al_{7.2}Si_{28.8}O_{72}] \times 18\,H_2O$ but X-ray crystal-structure analyses located only 56% of the chemically analysed Ag. The authors argued that the additional Ag might be statistically dispersed within the structural voids. However, the high atomic weight of Ag and our experience with other extra-framework cations incorporated into heulandite leave doubts about

this interpretation. To obtain a fully Na^+-exchanged heulandite crystal of similar size other authors [37] treated the sample 3 months at 150 °C (Na^+ and Ag^+ have corresponding radii). Thus we may speculate that complete Ag exchange only occurred at the rims but not in the centre of crystals.

The **HEU** framework has the topological symmetry $C2/m$ which may be lowered (Cm, $C2$, both monoclinic, or $C1$, $C\bar{1}$, both triclinic) due to a more ordered Si, Al distribution, e.g. caused by the growth mechanism of the natural crystal [25]. In a sample with heteroionic extra-framework occupants, such differences cannot easily be resolved. However, if heavy metal ions are incorporated into the structural voids of heulandite those ions prefer atomic sites close to Al tetrahedra and their high electron density acts as a probe for the 'true' symmetry of the crystal. The consequence of symmetry lowering is that symmetry equivalent extra-framework positions (e.g. the B-site) in space group $C2/m$ are no longer symmetry equivalent in low symmetry space groups and split into two sites e.g. B and B' where one site may be highly populated whereas the other site may be empty. Because all subgroups listed above have the same extinction rules for X-ray reflections, the true symmetry can only be recognised by a rigorous comparison of weak intensities with corresponding calculated structure factors in each space group. For this reason test refinements in each possible space group are necessary where the 'true' model shows the best fit.

2.2. The location of extra-framework cations

Essentially complete heavy metal exchange accompanied by structural investigation are published for Ag**HEU** [36], Cd**HEU** [37], Pb**HEU** [38], and Mn**HEU** [39]; partial exchange was found for Cu**HEU** [39,40], and only traces of Er^{3+} and La^{3+} were analysed for a Na**HEU** precursor phase treated for ≈3 month at 150 °C with 0.5 M (Er, La) chloride solution of pH 2.8 [41]. Subsequent structure refinement and electron microprobe analyses indicated almost complete loss of Na and uptake of oxonium (H_3O^+) combined with partial dealumination of the framework where Al migrated to extra-framework positions. Extra-framework Al prefers octahedral coordination either by H_2O or framework oxygen. Very low La^{3+} and Nd^{3+} uptake by heulandite was also confirmed by Misaelides et al. [42].

In the following paragraph we attempt to bring some systematic to the site preference of extra-framework heavy-metal ions in heulandite. In the hydrated form of heulandite (space group $C2/m$) we label the most prominent extra-framework cation sites by a letter indicating the A, B, or C channel and a subsequent number (Fig. 2). In a dehydrated state the tetrahedral rings may collapse, even tetrahedral connections may break and other connections may develop, and therefore different extra-framework sites become important. Because the C channel connects the A and B channel parallel to [1 0 0] and [1 0 2] essentially all extra-framework sites are also part of the C channel. For this reason we only assign the label 'C-site' to those cations on the border between A and B channels. In the A channel there are three potential cation sites. A1, on the mirror plane, bonds to 2–5 oxygen sites of the tetrahedral framework and various H_2O molecules in opposite direction. Cations of different size or degree of hydration may adjust their bonding distance to the framework by displacement either towards C or

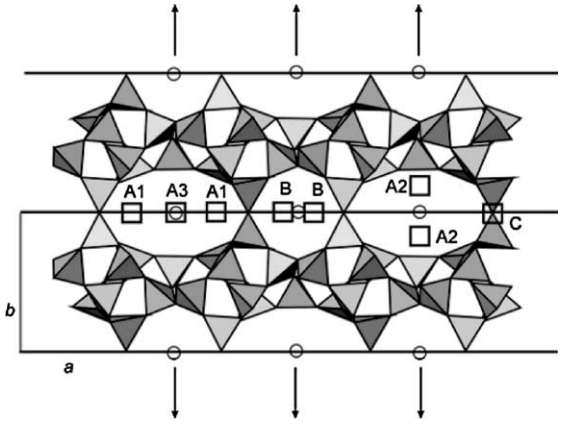

Fig. 2. Polyhedral model of a portion of the heulandite structure projected parallel to the c-axis with squares representing the most important extra-framework sites. In addition, the prominent symmetry elements for space group $C2/m$ are shown: small circles = centre of inversion, heavy horizontal lines = traces of mirror planes, double-barbed arrows = two-fold axes.

A3 (Fig. 2). A3 is in the centre of the A channel (in space group $C2/m$ positioned on the inversion centre). A3 has no bonds to the tetrahedral framework but is generally coordinated by only H_2O molecules (e.g. a $[M(H_2O)_6]^{2+}$ complex). Cations on A3 have in common that they show translational disorder parallel to c and rotational disorder of the H_2O complex approximately around the [2 0 3] direction. In particular, small cations prefer the A3 site. A2 is on the two-fold axis and has two bonds to adjacent oxygen sites of the framework with additional coordinating H_2O molecules opposite to it. For large cations, the B-site is on the mirror plane and exhibits up to four bonds to framework oxygen. Cations on the B-site may adjust their bonding distance to the framework by displacement towards the C-site, displacement along the c-axis, or by occupying a split position off the mirror plane. The various possibilities how cations may adjust their optimum bonding distance to the framework makes any prediction for preferred sites very difficult. Table 1 summarises the percentage of located cations on A1, A2, A3, B, and C for Ag**HEU**, Cd**HEU**, Pb**HEU**, Mn**HEU**, Cu**HEU** in addition to Sr**HEU** [39] and Na**HEU** [38] for comparison.

2.3. Cation disorder in the B channel

Starting from the precursor phase Na**HEU**, refined in space group $C2/m$ [38], two Na sites are generated by the two-fold axis, which have four H_2O molecules in common (Fig. 3). The Na–Na separation is 3.2 Å and Na bonds to three framework oxygen sites (1×2.55, 2×2.73 Å). The high Na occupancy of 84% indicates that adjacent Na positions must occur in the structure of Na-**HEU**.

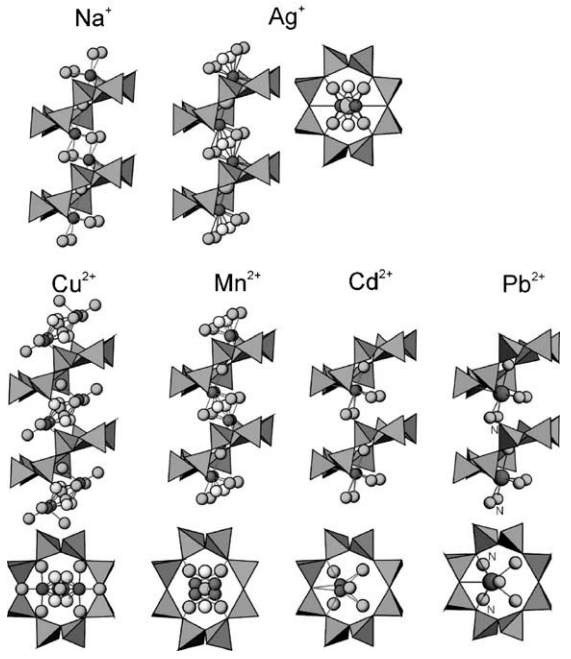

Fig. 3. Arrangement of extra-framework cations in the B channel. The eight-membered B-rings are seen edgewise, projected approximately parallel [0 1 0] and also along the c-axis. Dark grey spheres represent cations; light grey spheres are H_2O molecules. H_2O molecules marked 'N' for Pb**HEU** were not reported in the original study but were located in a recent re-investigation of the same crystal. Notice that in the view through the channel axis (parallel to c) Mn^{2+} and Cd^{2+} are displaced from the horizontal mirror plane.

If Na^+ is replaced by Ag^+ a very similar pattern is obtained for the B channel. However, only 43% of Ag^+ necessary for charge balance was located [36]. The resulting Ag–Ag separation is 3.4 Å. Ag

Table 1
Distribution of extra-framework cations on various channel positions

Sample [Ref.]	Octahedral ionic radius	A1	A2	A3	B (%)	C
Na**HEU** [38]	1.02	47%	Empty	Empty	44%	9%
Ag**HEU** [36]	1.15	56%	Empty	Empty	43%	Empty
Sr**HEU** [39]	1.18	54%	Empty	Empty	46%	Empty
Pb**HEU** [38]	1.19	49%	21%	Empty	30%	Empty
Cd**HEU** [37]	0.95	28%	16%	27%	48%	Empty
Mn**HEU** [39]	0.83	3%	Empty	50%	47%	Empty
Cu**HEU** [40]	0.73	Empty	6%	44%	49%	Empty

For definition of the sites A1, A2, A3, B, and C see Fig. 2.

bonds to three framework oxygen sites (1×2.60, 2×2.78 Å). Between two adjacent Ag sites there are six partly occupied and closely spaced H_2O positions, all within bonding distance (2.3–2.9 Å). However, it remains unclear which H_2O sites are actually associated with Ag and which H_2O positions are occupied when the Ag site is empty.

A completely different pattern (Fig. 3) appears for Cu^{2+} **HEU** [40] because Cu (occupancy: 39%) is not bonded to the tetrahedral framework and two adjacent Cu sites are generated by the two-fold axis. Cu has approximately planar four-fold coordination by H_2O. The exact bonding distances of Cu^{2+} are masked by the fact that the H_2O populations are significantly larger than the Cu population thus also H_2O not bonded to Cu^{2+} occurs on similar positions.

The arrangement of Mn^{2+} (occupancy: 19%) in the B channel of heulandite [39] is similar to Ag^{+}. However, due to the smaller ionic radius of Mn^{2+} it does not reside on the mirror plane but is slightly displaced from it leading to a split position with a Mn–Mn separation of 0.8 Å parallel to *b* (Fig. 3). This displacement from the mirror plane leads to only two bonds to the framework (1×2.28 and 1×2.35 Å). Bonds between Mn and H_2O molecules are ≈2.2–2.3 Å long. The structure of Mn^{2+} exchanged heulandite was refined in space group $C2/m$ [39] and for this reason the Mn site has a symmetry equivalent position produced by the two-fold axis, separated by 2.85 Å from the former. Short distance Mn–Mn interactions will not occur due to low Mn occupancy (19%).

The structure of Cd**HEU** was refined in space group *Cm* [37]. Similar to Mn^{2+}, Cd is displaced from the mirror plane and occupies (occupancy: 44%) a split position with a Cd–Cd separation of 0.5 Å. Cd has two bonds to the framework (1×2.43 and 1×2.45 Å) and is coordinated to five additional H_2O molecules with bonding distances between 2.2 and 2.7 Å. A potential Cd position produced by a pseudo-two-fold axis along *b* has only a very low occupancy of 5%.

A *Cm* refinement was also performed for Pb^{2+} **HEU** [38]. The arrangement of Pb^{2+} in the B channel is very similar to Cd but Pb (occupancy: 60%) resides on the mirror plane and has three bonds to the framework (1×2.64 and 2×2.76 Å) and additional five H_2O molecules are bonded to Pb within 2.48–2.62 Å. Notice that two of the five H_2O molecules were not resolved in the original study [38] but became apparent in a recent re-investigation of the same crystal (Fig. 3).

2.4. Cation disorder in the A channel

Small cations such as Cu^{2+} and Mn^{2+} prefer the A3-site in the A channel (Fig. 4) and are fully hydrated forming an octahedral $[M(H_2O)_6]^{2+}$ complex [39,40]. Cuprammine treated heulandite exhibits on A3 a square planar $[Cu(NH_3)_4]^{2+}$ complex with two additional more distant H_2O molecules, completing the Cu^{2+} coordination to an elongated octahedron [40]. The complexes on A3 are generally disordered along the *c*-axis and exhibit rotational disorder approximately around the [3 0 2] direction (Fig. 4). Cd in the A channel is disordered over various sites [37]. There still exists the Cd–H_2O complex, though in minor concen-

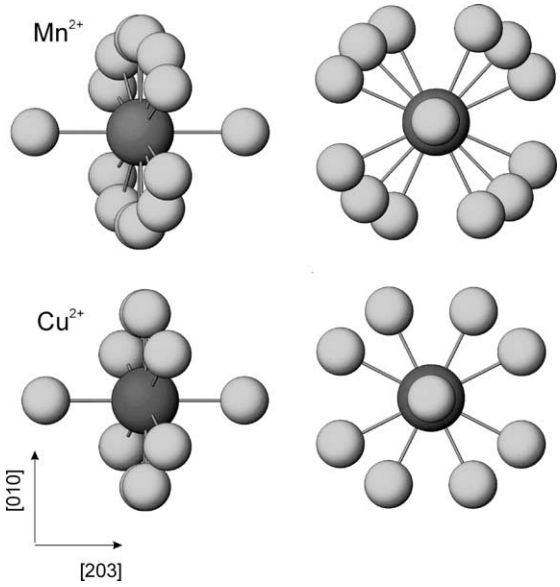

Fig. 4. Rotational disordered $[M(H_2O)_6]^{2+}$ complexes on the A3 site in heulandite. The figures to the left are projected parallel to the *c*-axis. The figures to the right are projections along [2 0 3] and display on overlay of three (Mn^{2+}) and two (Cu^{2+}) $[M(H_2O)_6]^{2+}$ complexes, respectively. Cations are represented by large, dark grey spheres; coordinating H_2O molecules are light grey.

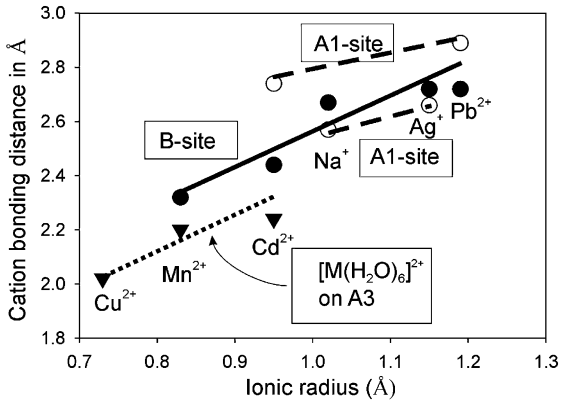

Fig. 5. Cation bonding distances of extra-framework metal ions. Dotted lines (triangles) represent metal-H_2O distances in the $[M(H_2O)_6]^{2+}$ complex; solid lines (filled circles) are average bond distances between the B-site and oxygen of the tetrahedral framework; dashed lines are mean bonding distances between the A1-site and oxygen of the tetrahedral framework.

tration. In addition, Cd occupies the A1 and A2 sites forming bonds to the tetrahedral framework. Pb was located only on A1 and A2 [38], whereas only the A1-site has been identified for Ag [36]. In contrast to expectation, the divalent cations Cd and Pb exhibit $\approx$0.2 Å longer distances to the framework than the monovalent cations Ag and Na (Fig. 5). This may indicate that Cd and Pb are strongly bonded to H_2O whereas bonds of Na and Ag to H_2O are considerably weaker.

3. Metal-forms (CoHEU, NiHEU, CuHEU, PdHEU, HgHEU, PbHEU, ThHEU, UHEU) studied by spectroscopic, thermal, and other techniques

3.1. CoHEU

The characterisation of natural pure **HEU**-type zeolites modified by Co (Co**HEU**) has been reported by Godelitsas et al. [43–45] regarding fully Na^+-exchanged (homoionic) crystal grains (20–90 μm) further treated with a 0.1 M $Co(CH_3COO)_2$ aqueous solutions at 100 °C. A similar procedure, though using more intense treatment conditions with 1 M $Co(CH_3COO)_2$ and 110 °C, was applied by Calligaris et al. [46] for the the preparation of the Co-form of pure **CHA**-type (chabazite) zeolite crystals. In the case of Co**HEU**, the RI–XRF measurements showed a rather high Co amount in the bulk, 7.5% (w/w). However, the SEM-EDS investigation revealed sub-microscopic Co-phases supported on the surface of the interacted zeolite, whereas a relevant study performed on polished-sections approved the intense metal accumulation around the rims of the grains with less concentrations in the interior. It is evident that the metal sorption is mainly attributed to surface precipitation of insoluble solid phases, due to hydrolysation of the initial Co^{2+}-ions, while incorporation of Co into the structure through the micropores also took place by ion-exchange. Detailed powder-XRD study approved that the pale-rose to brown layer covering the surface of the faintly-white zeolite grains is not crystalline corresponding to amorphous Co(III)-hydroxides and/or-oxyhydroxides. It should be mentioned that parallel experiments showed that typical bright-blue Co(II)-hydroxide, precipitated in aqueous solution, is crystalline and is further transformed at $\sim$150 °C to black crystalline Co(III)-oxide (the same black crystalline Co(III)-oxides precipitated on the surface of the zeolite upon treatment with $Co(CH_3COO)_2$ at 150 °C). Furthermore, the XPS study indicated the presence of Co(III)-hydroxides and/or-oxyhydroxides, which are hydrated according to TGA/DTG/DTA measurements showing a significant weight loss at lower temperatures not attributable to zeolitic water. The examination of the material obtained after thermal analyses up to 800 °C also confirmed that the pale-rose to brown amorphous Co(III) precipitates are finally transformed to black amorphous Co(III)-oxides. It is evident that, **HEU**-type zeolites modified by Co can be generally described as composite microporous materials with Co(III) phases supported on the surface of the Co-loaded zeolitic substrate (Fig. 6). Nevertheless, the above results lead to entirely different conclusions than those presented by Calligaris et al. [46] who argued that they prepared typical 'ion-exchanged' Co**CHA** crystals under similar experimental conditions. It should be noted that the sorption of Co mainly through adsorption and surface precipitation has also been shown by XPS and EXAFS for other natural

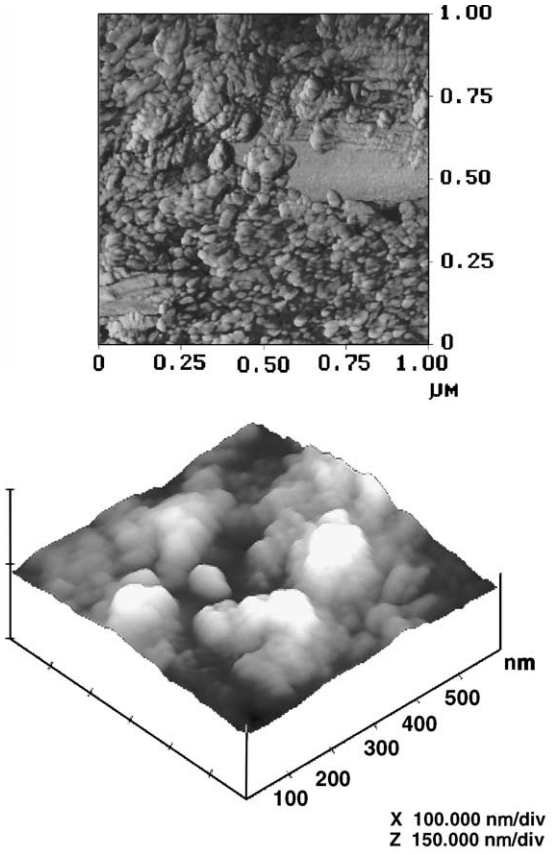

Fig. 6. Tapping mode AFM images of sub-microscopic Co precipitates on the heulandite (0 1 0) surface (crystal size 20–90 μm).

microporous materials such as kaolinite and goethite e.g. [47–49]. In the case of macroporous silicates like quartz, the phenomena are even more complicated with a possible formation of a Co layer-silicate growing epitaxially on the surface, topotactically on a surface amorphous layer, or independently of the quartz framework structure [50].

Data in respect of synthetic **HEU**-type zeolites modified by Co are available by Kim et al. [51] focussing on the selective reduction of NO by CH_4 in the presence of excess O_2 rather than on the characterisation of the materials. The metal-loaded samples were also prepared using $Co(CH_3COO)_2$ aqueous solutions at 80 °C, and further Co**HEU** was calcined (dehydrated) in air at 500 °C for 12 h. For comparison, other synthetic zeolites of the **MFI**-type (ZSM-5) and **FER**-type (ferrierite) modified with Co were prepared in the same way. According to the authors, at $T \geqslant 500$ °C, Co**HEU** is much more active for NO reduction than Co**MFI**, but it is less active than Co**FER**. Besides it is found that the selectivity for CH_4 toward reacting with NO at high temperatures ($T \geqslant 450$ °C) is higher on Co**HEU** than on Co**MFI** or Co**FER**. On the basis of the overall catalytic results, the importance of zeolite pore size as a structural parameter influencing the activity of intrazeolitic Co^{2+} ions for NO reduction by CH_4 is indicated throughout the paper. Concerning the above data, it should be noted that the typical characterisation of Co**HEU** by powder-XRD, N_2-BET and wet-chemical methods does not provide adequate information for the hypothesis that 'intrazeolitic Co^{2+} ions' are responsible for the observed catalytic behaviour. Moreover, the assignment of the solid acidity of Co**HEU**, measured by TPD of ammonia, only to 'intrazeolitic Co^{2+} ions' excluding other possible sorbed Co species and/or phases, could be subject of further discussion.

3.2. NiHEU

Natural **HEU**-type zeolite crystals modified by Ni (Ni**HEU**) were studied by Godelitsas et al. [44,52] after treatment with 0.1 M $Ni(NO_3)_2$ at 100 °C using the homoionic Na-form as precursor phase. The same procedure had been previously applied by de las Pozas et al. [53] for the Ni-modification of **HEU**-type zeolite bearing sedimentary rocks (tuffs). The total Ni content of the pale-green Ni-loaded **HEU**-type zeolite, determined by RI–XRF, was 3.5% (w/w) (35 mg/g). The calculated CEC of the precursor Na**HEU** zeolite (302 meq/100 g) strongly suggests that the fully Ni^{2+}-exchanged Ni**HEU** material could theoretically contain 88.62 mg/g Ni. However, if one assumes that Ni^{2+} ions had been sorbed through ion exchange, the product would primarily be a partially Ni^{2+}-exchanged (non-homoionic) zeolitic material. Bulk analyses of the material showed that a considerable amount of Na remained in the crystal structure of Ni**HEU**. SEM-EDS of polished sections of the material indicated that the

distribution of Ni was remarkably inhomogeneous throughout the grains, with significant accumulation towards the rims and around the edges. This means that the non-homoionic Ni**HEU** crystals were also non-stoichiometric, so the nickel sorption by the zeolite may not be completely attributable to ion-exchange. The XPS study showed that the near-surface layers of the material comprised not Ni^{2+} ions but specific compounds corresponding to hydroxides of Ni(II) (Ni $2p_{3/2}$ peak resolved at 856 eV). This is further supported by observation of an extra characteristic sharp band at 1384 cm^{-1} in the FT-IR spectra of Ni**HEU**, associated with the (OH) stretching vibrations of metal hydroxides and/or oxyhydroxides. These data are further verified by SEM-EDS investigation of individual Ni**HEU** crystals, indicating the presence of very small (up to 2 μm) solid nickel phases supported on the zeolite surface. In addition, the powder XRD study of Ni**HEU** and pure $Ni(OH)_2$ proved the crystalline nature of the surface nickel hydroxide phases by weak but well-resolved peaks in the corresponding diffraction patterns which were not due to the structure of the **HEU**-type zeolitic substrate. The Ni**HEU** zeolitic material is not a typical partially Ni^{2+}-exchanged (non-homoionic) form of a **HEU**-type zeolite, and the non-stoichiometric Ni-loaded crystals have possibly been formed through metal sorption mechanisms, which do not exclusively involve ion exchange. These mechanisms are mainly represented by distinct surface chemical processes, such as adsorption and surface precipitation, taking place at the solid-solution interface during treatment of the zeolite with aqueous solutions of Ni^{2+} ions. These processes are facilitated by the hydrolysis of the Ni^{2+} ion, which is favoured at the elevated temperature required for sufficient metal loading. As a result, various hydrolysis products interact progressively with the microporous solid, which can also act as a forceful cation exchanger. The positively charged solvated species, such as $[Ni(H_2O)]_n^{2+}$ and $[NiOH]^+$, are sorbed primarily through ion-exchange replacing initial extra-framework Na^+ ions, whereas mononuclear and/or polynuclear insoluble hydroxide species can be bonded to the material by surface precipitation. As a consequence, the Ni**HEU** zeolite exhibits a rather complicated structure in which Ni(II) ions occupying different sites in the micropores (channels) and on the surface possess differing Lewis and/or Brønsted acidic properties. As dipositive metal cations with small ionic radii are preferentially surrounded by H_2O molecules and are less coordinated by framework O atoms [39], in the Ni-loaded **HEU**-type zeolite Ni^{2+} ions with an ionic radius of 0.70 Å [31] are expected to be completely surrounded by H_2O molecules in the large micropores (A and B), probably without coordination by framework O atoms. The existence of hydrated Ni^{2+} ions in the structure of Ni**HEU** is further supported by the DR(UV/Vis) spectra showing a characteristic broad band in the 630–765 nm region and a band at 390 nm. However, the ^{29}Si and ^{27}Al MAS NMR spectra of Ni**HEU** are identical to those of the raw **HEU**-type zeolite, strongly suggesting that the aluminosilicate framework has not been affected by the sorption of Ni^{2+} ions. The Si/Al ratio of Ni**HEU** calculated from deconvolution of the ^{29}Si MAS NMR spectra is also the same (3.78). The Ni^{2+} ions encapsulated in the structure of Ni**HEU** introduce a weak solid acidity to the material that can easily be recognised after suitable thermal treatment (activation), which leads to the removal of the coordinated water molecules and the creation of Lewis acid sites due to the dehydrated Ni^{2+} ions. However, the Ni hydroxide phases supported on the surface of the crystals seem to play a more critical role in the solid acidity, for they tend to constitute Brønsted acid sites, adding stronger acidity to the nickel-loaded zeolite. The thermal analyses of Ni-**HEU** revealed a total weight loss of 15.93% involving three main stages, but complete dehydration of the crystals was realised below approximately 400 °C corresponding to a major weight loss of approximately 13%. A discrete endothermic event resolved in the DTA curve at 150 °C is evidently related to the release of zeolitic H_2O molecules predominantly associated with the Ni^{2+} ions in the micropores. The minor weight loss (2.93%) from approximately 400 to 800 °C could be attributed to dehydroxylation of the surface-supported nickel hydroxide phases, which was a potential source of volatile constituents that could be released at higher temperatures. The SEM-EDS

examination of the thermally treated Ni**HEU** showed that the grains obtained retained the external morphology of the initial zeolite crystals, but the powder XRD data indicated that the solid had become practically amorphous. However, careful evaluation of the powder XRD patterns revealed the presence of a small sharp peak, separated from the background, which corresponded to crystalline Ni(Al,Si) oxides. Partial re-crystallisation evidently takes place as a result of the progressive reaction of the dehydroxylated nickel hydroxide phases with the amorphous zeolitic substrate. These results imply that complete dehydration (activation) of Ni**HEU**, which is required for identifying the acid sites by TPD and in situ FT-IR/MAS NMR spectroscopy, can be achieved reasonably well at quite low temperatures (below approximately 400 °C). TPD of ammonia gave a considerable total solid acidity of Ni**HEU** (8.93 mg NH_3/g). The broad peak in the TPD pattern with a maximum at 183 °C corresponds to 'weak' acid sites, which are represented mainly by Lewis-type sites such as the dehydrated Ni^{2+} ions. Associated acid sites are also considered to be any relevant extra-framework species located in the micropores (that is, the residual Na^+ ions), including potential Al^{3+} ions in an octahedral coordination environment (Al^{oct}), which can be formed in activated zeolites. The second broad peak in the TPD profile, with a maximum at 461 °C, corresponds to 'strong' acid sites, which are primarily attributed to Brønsted-type sites containing protonated active groups. The characteristic Brønsted-type sites in the structure of activated zeolites are the so-called bridging hydroxyl groups, consisting of protons bonded to the aluminosilicate framework in the micropores (Si–O(H)–Al). However, possible silanol groups (Si–OH) commonly formed on the surface of zeolites (terminal hydroxyl groups) do not constitute 'strong' acid sites and are generally of minor importance. Extended bridging hydroxyl groups are usually created in NH_4^+-exchanged zeolites as a result of the release of NH_3(g) during the thermal treatment, but are not typical of metal-loaded zeolites. Therefore, in Ni**HEU** the 'strong' acid sites observed in the TPD pattern are probably due to the surface-supported Ni hydroxides. The different types of acid sites were characterised further by in situ FT-IR spectroscopy after exposure of the activated metal-loaded zeolite to gaseous strong electron donor ligands such as pyridine (Py). The FT-IR spectroscopy showed clearly that Py is chemisorbed on the activated Ni**HEU** zeolite through reaction with certain structural acid sites of the zeolite. The lack of discrete absorption bands in the 3700–3500 cm^{-1} region indicates the absence of Brønsted-type acid sites attributable to bridging hydroxyl groups. In contrast, some absorption bands appearing in the 1700–1400 cm^{-1} region strongly suggest that Py can also be chemisorbed to Lewis and/or Brønsted acid sites different from those of the bridging hydroxyl groups. The normal vibrational modes with maxima at 1610 cm^{-1} and 1447 cm^{-1} are due to the species resulting from the interaction of the lone-pair orbital of Py with the appropriate vacant orbital of the Lewis acid sites, whereas that at 1650 cm^{-1} is characteristic of the pyridinium ion formed by interaction of Py with the protons of the Brønsted acid sites. The band at 1491 cm^{-1} could be attributed to the pyridine ring and is common to all Py-containing species. These data substantiate the existence of strong Brønsted-type acid sites due to surface-supported Ni hydroxides, identified with certainty by a characteristic peak at 461 °C in the TPD pattern of Ni**HEU**. However, the Lewis-type acid sites, verified by FT-IR spectra of the Ni-**HEU**-Py material, could be primarily due to dehydrated Ni^{2+} ions located in the micropores, as well as to residual Na^+ ions. In addition, evidence for acid sites due to extra-framework octahedrally coordinated Al^{3+} ions was obtained from ^{27}Al MAS NMR spectra. The in situ ^{27}Al MAS NMR spectrum of Ni**HEU**-Py exhibits, besides the characteristic peak at 56 ppm due to tetrahedral Al (Al^{tet}) moieties, a second very broad peak at ~0 ppm possibly due to the presence of Al^{oct} moieties. However, the ex situ ^{27}Al MAS NMR spectra recorded after rehydration of the material (forming Ni**HEU**-Py/R) exhibited only the single peak at 56 ppm due to Al^{tet}; hence no real Al^{oct} moieties were created in order to remain in the rehydrated crystal structure. Consequently, distorted Al^{tet} PBUs are most probably formed in the aluminosilicate framework of the zeolite upon activation which

are further rearranged. The powder-XRD patterns of Ni**HEU**-Py/R also demonstrated that the crystal structure of the zeolite is essentially preserved during dehydration/activation followed by Py sorption and rehydration. A reversible structural transformation of this kind has not been reported previously for zeolites, but it is known for other microporous materials, such as the zeotype $AlPO_4$ [54]. Therefore, the Lewis-type acid sites resolved in the in situ FT-IR spectra are represented solely by exchangeable cationic species and particularly by the dominant Ni^{2+} ions. The structural, electronic, energetic and spectroscopic properties of all possible Ni(II) dihydroxyl and aqua complexes ($[Ni(OH_2)]_n^{2+}$ and $[Ni(OH_2)_{n-2}(OH)_2]$ where $n = 4$–6), absorbed through ion-exchange in the zeolite micropores or supported on the zeolite surface through adsorption/surface precipitation, were studied theoretically by density functional theory (DFT) calculations and discussed in relation to the above presented experimental data. According to the theoretical results the most likely species to be formed on the surface of the zeolite is the $[Ni(OH_2)_2(OH)_2]$ complex, thus substantiating the experimental spectroscopic properties (FT-IR and UV/Vis absorption spectra) of the Ni**HEU** zeolite. The computed proton affinities found in the 182.0–210.0 kcal/mol range, increase with increasing coordination number of the dihydroxyl and aqua Ni(II) complexes. It is evident that the above results unravel the data by de las Pozas et al. [53], who applied the same experimental conditions and argued about 'ion-exchanged' Ni**HEU** although they used a tuff with 85% **HEU**-type zeolite. The rather high metal-loading (1.1 meq/g, which means 32.3 mg/g or 3.23% w/w) can hardly be attributed solely to ion-exchange, excluding other sorption mechanisms as well as the contribution of other associated minerals.

Synthetic **HEU**-type zeolites ('clinoptilolite' powders) modified with Ni were investigated by Choo et al. [55] and by Choo and Kevan [56] using ESR (EPR) and ESEM spectroscopic techniques. In the first of the above papers, the synthesised Na(K)**HEU**-type zeolite was additionally ion-exchanged with Na^+ ions whereas Ni(II)-loaded samples were further obtained using a 0.5 mM $NiCl_2$ aqueous solution at 60 °C. The Ni(II) ions were introduced, according to the authors, into extra-framework sites through ion-exchange reactions. ESR spectroscopy and ESEM were finally used to study the formation of Ni(I) after thermal and hydrogen reduction, as well as various adsorbate interactions (with methanol, ammonia, CO, ethylene, butene and NO). Thermal reduction by dehydration at 300 °C shows a single species assigned to Ni(I) ions while two isolated Ni(I) ions are observed after hydrogen reduction at 350 °C. Adsorption of methanol on hydrogen-reduced Ni**HEU** forms a Ni(I)-$(CD_3OH)_n$ complex resulting from the interaction of methanol with one of the isolated Ni(I) ions. On the other hand, adsorption of ammonia produces a prominent Ni(I)-$(ND_3)_n$ complex by interaction with both Ni(I) ions. The ^{13}C hyperfine structure and ESEM analysis parameters after ^{13}CO adsorption indicate that Ni(I) interacts with one CO molecule and forms a Ni(I)-$(CO)_1$ complex. Two Ni(I)-$(C_2D_4)_n$ complexes are generated after adsorption of ethylene on dehydrated Ni**HEU** and subsequent heating below 350 °C. At higher temperature, these species disappear with the concomitant formation of two Ni(I)-$(C_4D_8)_n$ complexes, indicating ethylene dimerisation. ^2D ESEM confirms the coordination of Ni(I) with butene. Adsorption of NO on dehydrated Ni**HEU** produces two Ni(I)–NO^+ complexes formed by transfer of the odd electron from NO to Ni(II) ions. Along with two Ni(I)–NO^+ species. Another species assigned to the NO radical is also observed in Ni**HEU** after NO adsorption on both Ni**HEU** and Na(K)**HEU**. In the second paper [56], special attention was given to the catalytic activity and selectivity for ethylene dimerisation on Ni(II)-loaded samples (referred to Ni(II)-exchanged by the authors). It should be noted that the participation of H^+ ions in the structural formula of the zeolite is also referred in the experimental section. The ESR and catalytic results indicated that ethylene is dimerised to *n*-butenes at high temperature via direct reduction of Ni(II) by ethylene in Ni**HEU** containing different locations. Adsorption of ethylene on reduced Ni(I) sample at 25 °C led to the formation of Ni(0) clusters without any Ni(I) complexes with either ethylene or butene. This indicates that further reduction of Ni(I) occurs by

ethylene and no ethylene dimerisation occurs. The formation of *n*-butenes increases with the amount of Ni(II), but increased Ni(II) also causes faster deactivation due to formation of inactive Ni(0) clusters.

3.3. CuHEU

Natural **HEU**-type zeolites modified by Cu (Cu**HEU**) have been studied by Godelitsas et al. [44,57,59] and Misaelides et al. [58] mainly using a combination of spectroscopic techniques. The investigations concerned previously prepared homoionic Na**HEU** grains (20–90 μm) and raw Ca**HEU** platy fragments (2–5 mm), further treated with 0.1 M $Cu(CH_3COO)_2$ aqueous solutions at room temperature. The bluish, μm-sized crystals of CuHEU were particularly characterised by means of powder-XRD, SEM-EDS, RI–XRF, DR(UV–Vis), EPR, XPS, and EXAFS, while the mm-sized crystals were used for ^{12}C–RBS spectroscopic measurements. The bulk analyses of the Cu**HEU** grains by RI–XRF revealed that the modified zeolite contained 3.2% (w/w) Cu. However, point analyses of the material performed by SEM-EDS on free crystal surfaces showed that the Cu distribution in the crystals mass was exceptionally inhomogeneous. The highest Cu concentrations, up to 8.6% (w/w), were observed at certain regions of crystal faces other than the (0 1 0) cleavage plane. The irregular metal distribution was further verified by SEM-EDS profiles performed on polished crystal sections, showing a Cu enrichment around the rims of the grains; 0.4–2.4% at sections parallel to (0 1 0) and 0.1–3.5% at sections perpendicular to (0 1 0) hence the Cu**HEU** crystals were actually non-stoichiometric. Further analyses revealed a total Na content of 3.70% (w/w), compared to 6.95% of Na**HEU**, indicating that Cu-**HEU** was besides non-homoionic. The spatial distribution of Na was also proved irregular, with concentrations varying from 0.9% (w/w) on the surface up to 5.3% (w/w) in the interior of the crystals. The SEM data as related to detailed investigation of the powder-XRD patterns, suggest that the increased Cu concentration at the exterior of the crystals is not due to surface precipitation of Cu(II) phases such as hydroxides, oxyhydroxides, and oxides, unlike Ni**HEU** (see previous paragraphs). This is confirmed by the XPS spectra, in which the E_b of Cu $2p_{3/2}$ resolved at 935.5 eV strongly supports the absence of precipitated phases but the presence of Cu^{2+} ions coordinated with oxygen atoms of the aluminosilicate microporous material e.g. [60]. Therefore, the sorption of Cu by the **HEU**-type zeolite, though resulting in non-stoichiometric crystals, can principally be attributed to an ion-exchange mechanism. However, as noted above, a fully Cu^{2+}-exchanged (homoionic) form was not achieved. Less than 50% of the initial Na^+ exchangeable cations were replaced by Cu^{2+} cations, despite the efforts during the experimental work to remove as much Na as possible by continuous renewals of the Cu solutions and checking of the filtrates for Na using flame photometry. The inhomogeneous distribution of Cu in the interior of the crystals indicates an anomalous diffusion of Cu^{2+} ions into the **HEU**-type framework micropores, principally due to steric effects (related to inaccessible extra-framework sites) on metal ions participating in ion-exchange reactions. On the other hand, it seems that in some cases the distribution of the anionic charges in the zeolite structure is also inhomogeneous, and particularly near the surface of the crystals, affecting the sorption of metal cationic species from aqueous solutions. The study of the Cu-loaded larger fragments by ^{12}C–RBS also proved an elevated Cu accumulation in near-surface layers of the zeolite, with a total thickness of the metal-enriched region ~500 nm according to simulations by means of the relevant computer code RUMP. The RBS spectra concerned the (0 1 0) cleavage plane, chemically-modified by Cu, which is not connected to the network of channels of the zeolite structure. Thus the metal absorption on (0 1 0) could function through channels which terminate at faces other than the (0 1 0), or even by surface macro-defects (including cleavage macro-steps, and small fractures/cracks) and micro-defects (concerning micro-steps, kinks, and terrace vacancies). Indeed, the SEM-EDS investigation of both μm-sized and mm-sized Cu**HEU** crystals, showed the expected higher concentration of Cu in such surface discontinuities in a similar way to that observed by other authors in the case of Pb-loaded **HEU**-type

zeolites [38]. These surface defects can be explained in terms of structural regions with occasional 'destruction' of the entire aluminosilicate framework. This causes accumulation of delocalised negative charges as well as formation of surface secondary active sites (e.g. terminal OH-groups or Brønsted acid sites) favouring the sorption of metal ions at the solid–liquid interface. Moreover, in the case of the grains, taking into account the CEC of the precursor Na**HEU** zeolite (6.95% Na and thus 3.02 meq/g) we can suppose that a potential fully Cu^{2+}-exchanged Cu**HEU** material could theoretically contain 95.95 mg/g or 9.59% (w/w) Cu. Since the experimental product contained 3.70% Na and 3.2% Cu, it is evident that, during the sorption of Cu through ion-exchange reactions, ~1.42 meq of Na^+ were released in the solution while only ~1 meq of Cu^{2+} were introduced in the structure. All of the above results are in line with the data of Stolz and Armbruster [39], who also concluded that Cu^{2+}-exchanged **HEU**-type zeolite crystals showed rather complicated composition due to low Cu uptake in comparison with the large decrease of the initial Na content. In this case 4 M $CuCl_2$ solution of high acidity (pH = 0.70) was used to avoid surface precipitation of Cu-hydroxychlorides. The channel cation deficiency was considered to be compensated by the incorporation of H^+/H_3O^+ and minor amounts of Al^{3+} available from partial crystal dissolution under the intense acidic conditions (see previous paragraphs). Dissolution etch-pits were also observed by SEM on the surface of the Cu^{2+}-exchanged **HEU**-type zeolite crystals. In the case of the $Cu(CH_3COO)_2$-treated samples the pH was higher and accordingly no etch-pits were observed using SEM. Therefore, the effect of pH was minimised but the ion-exchange of minor amounts of H^+ cannot be excluded. In a recent study [41] on Cu-**HEU**, obtained by $Cu(CH_3COO)_2$ exchange of Na**HEU**, no Na could be detected in the exchange product but only 3.3 Cu^{2+} per formula unit were analysed, although ≈8.6 Al were present in the tetrahedral framework. The deficit of ≈2 positive extra-framework charges may be explained by H^+. Besides, although Al^{3+} cations were not likely available due to dissolution, the appearance of Frenkel-type intrinsic defects such as $Al^{tet} \Rightarrow Al^{oct}$ during metal-loading cannot be excluded as well. Nevertheless, it seems that either the unavoidable sorption of H^+ cations or the development of extra-framework sites occupied by Al^{3+} ions, are responsible for charge balance in Cu**HEU**. However, the investigation of the material by means of ^{27}Al MAS NMR for defining possible Al^{oct} should be a subject of further research. Although the existence of extra-framework Al^{3+} ions has not been approved spectroscopically yet, the DR(UV–Vis) spectra [59] are indicative of the presence of cupric ions in structure of Cu**HEU**. Accordingly, the EPR spectra, typical for Cu-loaded zeolites [61], and specifically the calculated g and A tensors ($g_\perp = 2.09$, $g_\parallel = 2.32$, $A_\perp \times 10^4 = 16\ cm^{-1}$, $A_\parallel \times 10^4 = 138\ cm^{-1}$) suggest Cu^{2+} ions in extra-framework sites of tetragonally distorted (4 + 2) octahedral coordination. The slightly higher G value, compared with that of cupric aquo-complexes, may be attributed to the immobilisation of the Cu^{2+} ions in certain chemically active sites of the solid material [62]. In addition, a weak signal at $g \sim 4.3$, which is characteristic of ferric ions, was also detected. This is due to minor tetrahedral Fe^{3+} from the raw **HEU** crystals, which was preserved, despite the chemical treatments, in Na-**HEU** and finally in Cu**HEU**. Finally, the EXAFS data approved the EPR-indicated structural environment around the Cu^{2+} ions which are surrounded by six oxygen atoms in the first shell (radius = 1.88(2) Å) whereas the second- and third-neighbour shells involve again Cu^{2+}. In particular the EXAFS results strongly support the argument that the material contains small 'CuO' clusters. These 'CuO' clusters can be considered as structural units of the Cu**HEU** lattice and not as distinguished clusters of Cu(II)-oxide phases. For the latter, the Cu–O distance has been found to be higher, in the range 1.96–2.78 Å [63]. These observations imply that the HEU-type zeolite structure can act as a polydentate σ-donor ligand providing the Cu^{2+} ions with a tetragonally distorted octahedral environment involving highly covalent Cu–O bonds. However, the formation of a $Cu–O_6$ chromophore would not be expected, hence one and/or two of the six coordinated oxygen atoms might be extra-framework electron donor atoms belonging to H_2O molecules.

Obviously, the H_2O molecules can be substituted nucleophilically by other stronger-donor ligands, such as $(C_2H_5)_2$ NCS_2^- at surface structural sites. In this case mixed-ligand coordination compounds supported on the **HEU**-type zeolite are formed, with both Cu–O and Cu–S coordination bonds in a novel type of coordination sphere around the Cu^{2+} ions [59].

Extended investigation of Cu-modified **HEU**-type zeolites using EPR (ESR) and ESEM measurements, was performed for synthetic samples ('clinoptilolite' powders) previously converted to the H- and several alkali (Li,Na,K)-forms and further treated with $Cu(NO_3)_2$ solutions [64]. In addition, the Cu-loaded materials (referred by the authors as 'fresh' samples doped with Cu^{2+}) were either calcined or interacted with polar molecules such as water, ammonia, alcohols, and acetonitrile. In general, strong effects of the H^+, Li^+, Na^+, and K^+ co-cations have been found on the coordination number and on the location of the cupric ion. Cu^{2+} coordinates three H_2O molecules in hydrated (Cu,H)**HEU** and in (Cu,Li)**HEU**, but only two H_2O molecules in hydrated (Cu,Na)**HEU** and (Cu,K)**HEU**. Two cupric ion sites are observed in many cases and are attributed to extra-framework sites in ten-ring (A-type) and eight-ring (B-type) channels. Activation to 400 °C is sufficient to remove these water molecules and cause migration of Cu^{2+} to an eight-ring intersecting channel. Interaction with polar molecules causes the migration of Cu^{2+} into the main channels to coordinate with the adsorbates. Cu^{2+} forms complexes with three molecules of ethanol and four of ammonia in (Cu,H)**HEU**, but only coordinates to two molecules of ethanol or methanol and three of ammonia in (Cu,Na)**HEU**, and to one molecule of ethanol or methanol and three of ammonia in (Cu,K)**HEU**. Cu^{2+} coordinates four molecules of acetonitrile at the centre of a main channel and this coordination number is unaffected by the alkali metal locations.

3.4. PdHEU

Concerning **HEU**-type zeolites modified by Pd, experiments and spectroscopic studies have been performed up to now only for synthetic samples according to Choo et al. [65,66]. In the first paper, Pd(II) in (Pd,Na,K)**HEU** zeolite (white in color) is introduced into extra-framework sites as $[Pd(NH_3)_4]^{2+}$ by liquid-state ion-exchange at 25 °C, whereas in (Pd,H)**HEU** zeolite (brown in color) is incorporated by solid-state ion-exchange at 550 °C using $Pd(NH_3)_4Cl_2 \cdot H_2O$. Dehydration at 200 °C produces one Pd(I) species in (Pd,H)**HEU** but no ESR signal in (Pd,Na,K)**HEU**, indicating that the stability of Pd(I) between the two materials is different, probably due to the different locations and environments of Pd in these systems. Hydrogen reduction of Pd(II) in these two materials after activation reveals that Pd(II) ions in (Pd,Na,K)**HEU** occupy relatively accessible sites in comparison to those in (Pd,H)**HEU**. The interactions of Pd(I) formed by thermal reduction of (Pd,H)**HEU** with various adsorbates were also studied. The ESR studies coupled with ESEM measurements show that Pd(I) in (Pd,H)**HEU** interacts rapidly with molecules smaller than methanol, such as hydrogen, water, ammonia, and carbon monoxide, and forms stable complexes. However, adsorption of benzene and pyridine on thermally reduced (Pd,H)**HEU** produces no ESR signal due to a Pd(I)-benzene complex or a Pd(I)-pyridine complex, suggesting that Pd(I) is located at a site in eight-ring (B-type) channels where benzene and pyridine are too bulky to enter. The second paper [66] concerning (Pd,H)**HEU** and other synthetic zeolites with different channel systems, focuses on the study of their catalytic activity for ethylene dimerisation. Besides it is indicated that thermal and hydrogen reduction of Pd(II) in all zeolites produce isolated Pd(I) with somewhat different ESR parameters. Regarding **HEU**-type materials, it has been shown experimentally that dehydrated H**HEU** exhibits no ethylene dimerisation activity whereas (Pd,H)**HEU** has catalytic activity if a thermally reduced sample containing Pd(I) is exposed to 0.13 bar of ethylene at 25 °C and is then annealed at 80 °C for various reaction times. This suggests that Pd(I) participates in the formation of active sites. Moreover, about 20% of the initial ethylene is converted to *n*-butene in (Pd,H)**HEU** with $Pd/Al = 0.12$. It should be noted that the study of Choo et al. [66] is closely related to a previous one about the catalytic activity and

selectivity for ethylene dimerisation on Ni(II)-loaded samples [56]. Nevertheless, both investigations demonstrate the importance of catalysts based on **HEU**-type zeolites modified by transition elements, and specifically by platinum-group elements (PGE), promising crucial industrial applications.

3.5. HgHEU

Data concerning **HEU**-type zeolite crystals modified by Hg have been presented by Misaelides et al. [58,67] and Misaelides and Godelitsas [68], for μm-sized homoionic Na**HEU** grains and raw mm-sized Ca**HEU** fragments derived from natural samples. In both cases the precursor materials were treated with $Hg(CH_3COO)_2$ aqueous solutions, and the subsequent investigation of the metal sorption processes was performed mainly using radioanalytical (RI-XRF, ^{197}Hg or ^{203}Hg and γ-ray spectrometry) and accelerator-based (^{12}C-RBS) spectroscopic techniques. In the case of the Na**HEU** grains, the initial Hg concentration in the aqueous solutions varied between 10 and 20 000 mg/l. The sorption of Hg by the material (in mg/g) was found to be significant, depending on the initial concentration, but the distribution coefficient values K_d (in ml/g) were remarkably increased between 25 and 100 mg/l. As it was expected, the interaction between the zeolite and dissolved Hg(II) was shown to be related to different sorption mechanisms including ion-exchange, adsorption, and surface precipitation. SEM-EDS profiles on polished-sections of the metal-loaded grains revealed the existence of absorbed (ion-exchanged) Hg in the interior of the crystals and much higher metal concentrations around the rims. The excessive Hg accumulation on the surface of the modified zeolite can undoubtedly be attributed to intense adsorption and surface precipitation of hydrolysis products. It is well-known that Hg^{2+} cations are exceptionally unstable, and they are easily hydrolysed in aqueous solutions [33]. These phenomena were finally confirmed by means of ^{12}C-RBS, performed on the mm-sized samples which were exposed for 24 h in a solution containing 1000 mg/l Hg. The ^{12}C-RBS spectra, according to RUMP simulations, revealed an 130 nm thick surface 'layer' enriched in Hg due to adsorption and surface precipitation. The nature of the Hg-modified surface was also investigated using XPS, which indicated the presence of Hg(II) oxide and/or hydroxide species (Hg $4f_{7/2}$ photopeak at 101.4 eV). The above results demonstrate the great difficulty to achieve fully or even partially Hg^{2+}-exchanged **HEU**-type zeolites.

3.6. PbHEU

As mentioned before (see previous paragraphs), the crystal structure of fully Pb^{2+}-exchanged **HEU**-type crystals was determined by Gunter et al. [38]. In this case, small (100–500 μm) Na**HEU** fragments were treated for 3 weeks with 2 M $Pb(CH_3COO)_2$ at 100 °C. Furthermore, Misaelides et al. [58] elaborated ^{12}C-RBS spectroscopic measurements on larger (2–5 mm) Ca**HEU** fragments treated for 24 h with 1000 mg/l Pb at room temperature. The RBS data verified a significant Pb accumulation in the near-surface layers of the material (thickness 130 nm) due to a possible anomalous diffusion of Pb^{2+} cations into the micropores during ion-exchange. The results revealed in fact that the short-time treatment of the larger crystals which were not NaCl-pretreated under ambient T conditions, leads to inhomogeneous Pb distribution. It is therefore confirmed that the modification of **HEU**-type zeolites by interaction with heavy metals in aqueous solutions strongly depends on the size of the crystals, the type of the zeolitic exchangeable cations, the treatment time, and the temperature.

3.7. (Th,U)HEU

The investigation of pure **HEU**-type zeolite crystals interacted with actinides, and namely with Th and U, was presented by Vochten et al. [69], Misaelides et al. [58], and Godelitsas et al. [70,71] for natural samples. In the first of the above papers zeta-potential measurements were used to illustrate the effect of pH on the sorption of uranyl ions (5×10^{-5} M) contained in phosphoric-buffered solutions by untreated Ca**HEU** specimens. The results indicated that the metal sorption takes place mainly through binding of hydrolysis

products on the crystal surface. Further experimental work [70], concerned the interaction of homoionic Na**HEU** grains (20–90 μm) and powders (<20 μm) with unbuffered U solutions of concentration between 50 and 20 000 mg/l at room temperature. However, only the fine-grained material was studied in detail since it was found to sorb much higher amounts of the metal than the coarse-grained material. The characterisation of the U-loaded samples was performed by means of Instrumental Neutron Activation Analysis (INAA) combined with high-resolution γ-ray spectrometry, RI-XRF, FT-IR, SEM-EDS, and powder-XRD. The sorption of U was found to be rather low in respect of the CEC of Na**HEU**. If we suppose that only UO_2^{2+} ions could be sorbed through ion-exchange, then the material should theoretically be loaded with a maximum of ~408 mg/g UO_2^{2+} or ~360 mg/g U. The experimental results showed bulk U concentrations in the modified solids between 2.84 and 11.68 mg/g. Besides the K_d values were found to be up to 190.59 ml/g for the solution of U concentration 100 mg/l, indicating that the best metal removal achieved was equal to 48.6%. On the other hand, the amounts of Na released from the structure of the zeolite were found to be comparably elevated in all cases. The sorption of H^+ ions, as it is derived by the increase of the initial pH values (from $pH_{initial} = 2.78–4.87$ to $pH_{final} = 3.04–6.39$), was also significant. At this point it should be noted that the initial unbuffered U aqueous solutions, prepared by dissolving $UO_2(NO_3)_2 \cdot 6H_2O$ in doubly-distilled water, were found to be naturally acidic with pH values directly correlated to the corresponding U concentration ($pH_{initial} = 6.5897[U]_{initial}^{-0.0883}$, $R^2 = 0.987$). It is evident that the sorption of H^+ along with the simultaneous release of Na^+ comprise chemical processes taking place in parallel, while the sorption of U occurs rather independently (Fig. 7). These parallel chemical processes are most probably due to ion-exchange reactions, and they can adequately be described by the general function (H-sorbed) or (Na-released) $= a[U]_{initial}^{b}$ ($R^2 > 0.9$) where a and b are numerical factors. On the other hand, the sorption of U is more complicated due to both the aqueous chemistry of the element and the properties of the

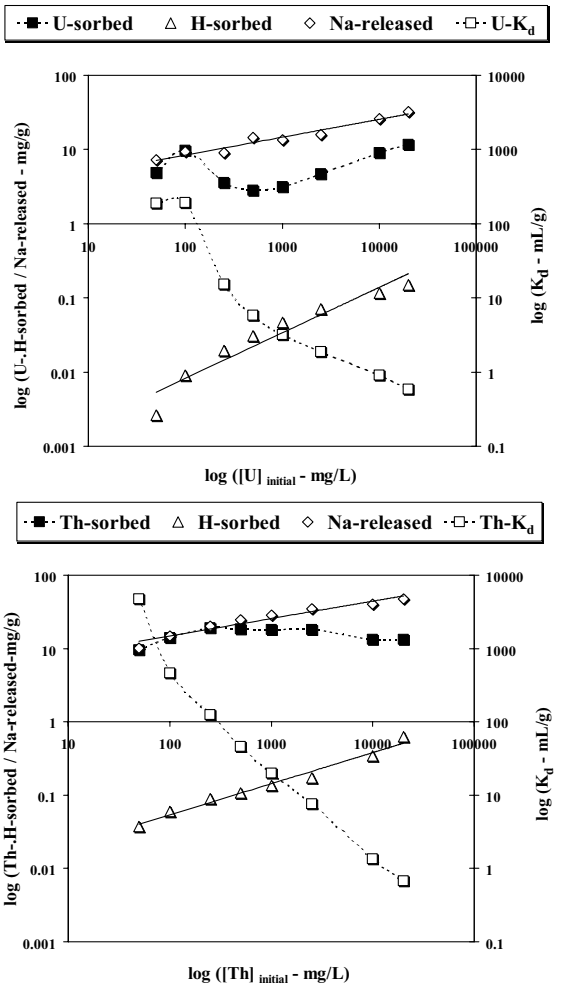

Fig. 7. Schematic illustration of data concerning the interaction of homoionic Na**HEU** powdered crystals (particles-size <20 m) with U (upper) and Th (lower) aqueous solutions of metal concentrations between 50 and 20 000 mg/l [70,71]. The sorption distribution coefficients K_d ($K_d = \frac{C_s}{C_w}$, where C_s is the concentration in the solid and C_w is the concentration in the aqueous solution) describe the distribution of the elements (U, Th) between the zeolite and solution, independently from the mass of the solid [34]. K_d = distribution coefficient.

microporous solid gradually modified during the interaction. In aqueous solutions of $pH < 4$ the most dominant species is the hydrated uranyl ion $[UO_2(H_2O)_6]^{2+}$ exhibiting a hexagonal bipyramidal structure with the U atom at the centre. At higher pHs it is readily hydrolysed towards a variety of hydrolysis products of the general type

$[(UO_2)_x(OH)_y]^{(2x-y)+}$. Hydrolysis is accelerated by the presence of the zeolite which preferentially sorbs H^+ ions and subsequently increases the initial pH. For solutions of high U concentrations ($[U]_{initial} > 1000$ mg/l) the initial and final pHs are lower than 4, hence hydrolysis was rather restricted, and the sorption of U may be attributed to ion-exchange of UO_2^{2+} ions and other species such as $[UO_2(OH)^+]$. The powder-XRD investigation proved that all the zeolite samples retained their crystallinity after the treatment with the most acidic U solutions, whereas the SEM observations showed the absence of eroded or degraded crystals. However, the FT-IR spectra revealed remarkable dealumination phenomena based on the shift at higher frequencies of the main absorption band due to the asymmetric internal T–O stretching vibrations of the PBU. This indicates that the CEC of the zeolite is gradually reduced during the interaction, and besides Al^{3+} ions are most probably available (together with the UO_2^{2+} species and the H^+ ions) to compensate the extra-framework deficit related to the large decrease of the initial Na content. In the case of solutions of low U concentrations ($[U]_{initial} < 250$ mg/l) the initial and final pHs are higher than 4, and the sorption of U can mainly be explained on the basis of adsorption and surface precipitation mechanisms. Indeed, the examination of the corresponding modified zeolite samples by SEM-EDS confirmed that distinct U precipitates were deposited onto the surface of the crystals. Detailed powder-XRD analysis gave evidence for small but well-defined peaks attributed to hydrous U oxides of the type $UO_3.\times H_2O$. The argument for the presence of such crystalline phase on the surface of **HEU**-type zeolites modified with U was fortified by XPS [58], in the case of the mm-sized Ca**HEU** crystals, taking into account the U $4f_{7/2}$ photopeak [72] at 381.5 eV. Besides, the ^{12}C–RBS spectra strongly indicated the existence of a U-rich surface 'layer' of about 250 nm thickness due to adsorption and surface precipitation. Similar phenomena have also been described for U-loaded synthetic zeolites [73]. Moreover, Wersin et al. [74] studying the interaction between typical macroporous materials (Pb and Fe sulfides, i.e. galena and pyrite) and aqueous U solutions, proved an inhomogeneous U sorption at the surface of the crystals in the form of very small precipitates of U oxide compounds. The existing data concerning fine-grained **HEU**-type zeolite crystals (homoionic Na**HEU**, particles-size <20 μm) interacted with Th aqueous solutions [71] are also summarised in Fig. 7. In this case, the Th solutions of concentrations between 50 and 20 000 mg/l were found to be more acidic than those of U ($pH_{initial} = 5.2089[Th]_{initial}^{-0.0846}$, $R^2 = 0.985$). As a consequence, the zeolite sorbed considerable amounts of H^+ and the low pHs increased (from $pH_{initial} = 2.16$–3.72 to $pH_{final} = 2.42$–5.56). The sorption of H^+ as well as the release of Na^+ seem to be, as in the case of U, parallel chemical processes due to ion-exchange reactions as a function of $a[Th]_{initial}^{b}$. The distribution coefficients K_d appear comparably significant, approaching the value of 4780 ml/g for the solution of initial concentration 50 mg/l (metal removal 95.6%). The entire Th sorption can also be considered remarkable (up to 19.26 mg/g), though much lower of the theoretical maximum of 175 mg/g, taking into account the four-valent oxidation state of the Th. The enhanced reactivity of Na**HEU** is evident since experiments performed on macroporous tectosilicates such as quartz and feldspars showed negligible sorption of Th [75], whereas microporous layer-silicates with ion-exchange properties, such as biotite, sorbed up to 4.52 mg/g Th [76]. The hydrolysis of the Th^{4+} ion is intense in aqueous solutions of $pH > 3$, yielding a series of hydrolysis products of the general type $[Th_x(OH)_y]^{(4x-y)+}$. Therefore, in solutions of $pH < 3$ the aquathorium ion dominates, along with other minor species including $[ThOH]^{3+}$, and could be absorbed by the **HEU**-type structure. However, the accessibility to certain extra-framework sites through the channels is under question; according to Marcus [32] the Th ionic radius in aqueous solutions is ~1.13 Å and the Th–O(H_2) internuclear distance is 2.53 Å, but the exact hydrated ionic radius can hardly been evaluated because the number of the coordinated H_2O molecules depends on the solution and, in addition, the H_2O molecules near an ion are packed closer than they are in liquid water at room temperature. Nevertheless, the comparably large Na^+ release recorded in solutions of initial and final

pHs lower than 3 ($[Th]_{initial} > 2500$ mg/l) suggests that Th^{4+} ions are incorporated into the structure besides to H^+ ions. At the same time, the FT-IR spectra showed that dealumination takes place, as in the case of U, providing with extra-framework Al^{3+} ions. At this point it should be emphasised that, the dealumination phenomena which are observed at **HEU**-type zeolites interacted for rather short-time with acidic solutions, concern the near-surface layers of the materials (surface dealumination related to partial amorphisation) while most of the mass of crystals remains unaffected [77]. In the case of solutions of lower Th concentrations ($[Th]_{initial} < 500$ mg/l) the initial and final pHs are higher than 3, thus adsorption and surface precipitation should occur. The SEM-EDS and the powder-XRD investigations proved that Th discernible precipitates were supported onto the surface of the crystals corresponding reasonably to Th hydroxides which are white, gelatinous, amorphous substances in contrast to Th oxides which are typical crystalline phases with characteristic XRD peaks. The essential role of surface sorption mechanisms for pure **CHA**-type zeolite crystals (chabazite) interacted with Th aqueous solutions has been discussed by Misaelides and Godelitsas [78] and for synthetic zeolites by Sinha et al. [79]. Finally, one should mention that all the above results indicate the great difficulty to obtain fully or even partially Th^{4+}-exchanged **HEU**-type zeolites.

4. Perspectives for future research

According to the data reviewed above, there are wide perspectives for future research, mostly related to other common transition elements of environmental and industrial significance such as V, Fe, and Zn, as well as to the very interesting PGE including Pd which was recently studied in synthetic **HEU**-type zeolite samples [65,66]. The study of Fe is important for natural crystals, specifically in order to clarify oxidation state on extra-framework sites. The presence of Fe^{3+} ions on framework (tetrahedral) sites is well-known, even on the basis of spectroscopic investigations performed on single crystals e.g. [80]. In addition, relevant spectroscopic data e.g. [81] indicated Fe^{3+} ions in the channels as well as strong interferences due to micro-inclusions of hematite or $(Fe_{1-x}Al_x)_2O_3$ and small quantities of Fe sulfides (marcassite). On the other hand, spectroscopic investigations concerning raw, chemically- and thermally-modified **HEU**-type zeolites in zeoliferous rocks e.g. [82–84] lead to rather undecided results especially for the existence of non-framework Fe^{3+} in the structure. At the same time it is referred that paramagnetic Fe(III) commonly found in natural samples, limit their application as catalyst and its precise characterisation by spectroscopic techniques e.g. [65]. Finally, further research is necessary towards the interaction of pure **HEU**-type zeolite crystals with transuranic actinides such as Pu, for the better understanding of data already obtained in respect of relevant zeoliferous rocks e.g. [85–87].

References

[1] G. Gottardi, E. Galli, Natural Zeolites, Springer-Verlag, Berlin, 1985.
[2] B. Mason, L.B. Sand, Am. Mineral. 45 (1960) 341.
[3] F. Mumpton, Am. Mineral. 53 (1960) 1120.
[4] J.R. Boles, Am. Mineral. 57 (1972) 1452.
[5] D.B. Hawkings, Contr. Mineral. Petrol. 45 (1974) 27.
[6] A. Alietti, Am. Mineral. 57 (1972) 1448.
[7] L.D. Filizova, G.N. Kirov, V.B. Vassilenko, Compt. Rend. Acad. Bulg. Sci. 25 (1972) 1081.
[8] A. Alietti, M.F. Brigatti, L. Poppi, N.J. Mineral. Monatsh. (1977) 493.
[9] G.P. Valueva, Russian Geol. Geophys. 35 (1994) 1.
[10] D.S. Coombs, A. Alberti, T. Armbruster, G. Artioli, C. Colella, E. Galli, J.D. Grice, F. Liebau, J.A. Mandarino, H. Minato, E.H. Nickel, E. Passaglia, D.R. Peacor, S. Quartieri, R. Rinaldi, M. Ross, R.A. Sheppard, E. Tillmanns, G. Vezzalini, Can. Mineral. 35 (1997) 1571.
[11] D.L. Bish, J.M. Boak, in: D.L. Bish, D.W. Ming (Eds.), Natural Zeolites: Occurrence, Properties, Applications, Mineral. Soc. Am. Rev. Mineral. Geochem. 45 (2001) 207–216.
[12] E. Passaglia, R.A. Sheppard, in: D.L. Bish, D.W. Ming (Eds.), Natural Zeolites: Occurrence, Properties, Applications, Mineral. Soc. Am. Rev. Mineral. Geochem. 45 (2001) 69–116.
[13] Ch. Baerlocher, W.M. Meier, D.H. Olson, Atlas of Zeolite Framework Types, fifth ed., Elsevier, Amsterdam, 2001.
[14] S. Khodabandeh, S. Davis, Micropor. Mater. 9 (1997) 149.
[15] C.D. Williams, Chem. Commun. (1997) 2113.
[16] D.Y. Zhao, K. Cleare, C. Oliver, C. Ingram, D. Cook, R. Szostak, L. Kevan, Micropor. Mesopor. Mater. 21 (1998) 371.

[17] D. Zhao, R. Szostak, L. Kevan, J. Mater. Chem. 8 (1998) 233.
[18] D.W. Breck, Zeolite Molecular Sieves: Structure, Chemistry and Use, Wiley, New York, 1974.
[19] R.M. Barrer, Zeolites and Clay Minerals as Sorbents and Molecular Sieves, Academic Press, London, 1978.
[20] J. Griffiths, Ind. Miner. 87 (1987) 19.
[21] A. Dyer, Zeolite Molecular Sieves, Wiley, Chichester, 1988.
[22] G.V. Tsitsishvili, T.G. Andronikashvili, G.N. Kirov, L.D. Filizova, Natural Zeolites, Ellis Horwood, Chichester, 1992.
[23] H. Minato (Ed.), Natural Zeolite and its Utilisation, Tokyo, 1994.
[24] P. Misaelides, F. Macasek, T. Pinnavaia, C. Colella (Eds.), Natural Microporous Materials in Environmental Technology, Kluwer, Dordrecht, 1999.
[25] Th. Armbruster, in: A. Galarneau, F. Di Renzo, F. Fajula, D. Vedrine (Eds.), Zeolites and Mesoporous Materials at the Dawn of the 21st Century, Stud. Surf. Sci. Catal., vol. 135, Elsevier, Amsterdam, 2001, pp. 13–27.
[26] J.V. Smith, Chem. Rev. 88 (1988) 149.
[27] J.V. Smith, in: P.A. Jacobs, R.A. van Santen (Eds.), Zeolites: Facts, Figures, Future, Stud. Surf. Sci. Catal., vol. 49A&B, Elsevier, Amsterdam, 1989, pp. 29–39.
[28] H. van Koningsveld, in: H. van Bekkum, P.A. Jacobs, E.M. Flanigen, J.C. Jansen (Eds.), Introduction to Zeolite Science and Practice, Stud. Surf. Sci. Catal., vol. 58, Elsevier, Amsterdam, 1991, pp. 35–48.
[29] Th. Armbruster, M.E. Gunter, in: D.L. Bish, D.W. Ming (Eds.), Natural Zeolites: Occurrence, Properties, Applications, Mineral. Soc. Am. Rev. Mineral. Geochem. 45 (2001) 1–67.
[30] R.T. Pabalan, F.P. Bertetti, in: D.L. Bish, D.W. Ming (Eds.), Natural Zeolites: Occurrence, Properties, Applications, Mineral. Soc. Am. Rev. Mineral. Geochem. 45 (2001) 453–518.
[31] E.R. Nightingale, J. Phys. Chem. 63 (1959) 1381.
[32] Y. Marcus, Chem. Rev. 88 (1988) 1475.
[33] C.F. Baes Jr., R.E. Mesmer, Hydrolysis of Cations, R.E. Krieger Pub. Co. Inc., Malabar, 1986.
[34] W. Stumm, Chemistry of the Solid–Water Interface, Processes at the Mineral–Water and Particle–Water Interface in Natural Systems, J. Wiley & Sons Inc., New York, 1992.
[35] G.E. Brown Jr., G.A. Parks, P.A. O'Day, in: D.J. Vaughan, R.A.D. Pattrick (Eds.), Mineral Surfaces, Mineral. Soc. Series, vol. 5, Chapman & Hall, London, 1995, pp. 129–183.
[36] N. Bresciani-Pahor, M. Calligaris, G. Nardin, L. Randaccio, J.C.S. Dalton, (1981) 2288.
[37] J. Stolz, P. Yang, T. Armbruster, Micropor. Mesopor. Mater. 37 (2000) 233.
[38] M.E. Gunter, T. Armbruster, T. Kohler, C.R. Knowles, Am. Mineral. 79 (1994) 675.
[39] J. Stolz, T. Armbruster, in: C. Colella, F.A. Mumpton (Eds.), Natural Zeolites for the Third Millenium, De Frede-Editore, Naples, 2000, pp. 119–138.
[40] T. Armbruster, P. Simoncic, N. Döbelin, A. Malsy, P. Yang, Micropor. Mesopor. Mater. 57 (2003) 121.
[41] T. Wüst, J. Stolz, T. Armbruster, Am. Mineral. 84 (1999) 1126.
[42] P. Misaelides, A. Godelitsas, S. Harissopoulos, I. Anousis, J. Radioanal. Nucl. Chem. 247 (2001) 325.
[43] A. Godelitsas, J. Dwyer, D. Charistos, G. Manos, C. Tsipis, A. Filippidis, C. Hadjikostas, P. Misaelides, in: G.N. Kirov (Ed.), Abstracts of Sofia Zeolite Meeting '95, Sofia/BG, 1995.
[44] A. Godelitsas, J. Dwyer, D. Charistos, A. Filippidis, C. Tsipis, in: R. Catlow (Ed.), Abstracts of NATO-ASI on New Trends in Materials Chemistry, Il Ciocco/I, 1995.
[45] A. Godelitsas, D. Charistos, C. Tsipis, P. Misaelides, A. Filippidis, M. Schindler, Micropor. Mesopor. Mater., this volume. [doi:10.1016/S1387-1811(03)00356-1].
[46] M. Calligaris, G. Nardin, L. Randaccio, Zeolites 4 (1984) 251.
[47] J.G. Dillard, M.H. Koppelman, J. Colloid. Interf. Sci. 87/1 (1982) 46.
[48] C.V. Schenk, J.G. Dillard, J.W. Murray, J. Colloid. Interf. Sci. 95/2 (1983) 398.
[49] P.A. O'Day, G.A. Parks, G.E. Brown Jr., Clays Clay Mineral. 42/3 (1994) 337.
[50] A. Manceau, M. Schlegel, K.L. Nagy, L. Charlet, J. Colloid. Interf. Sci. 220 (1999) 181.
[51] Y.G. Kim, Y.C. Kim, S.B. Hong, M.H. Kim, Y.P. Kim, Y.S. Uh, Catal. Lett. 57 (1999) 179.
[52] A. Godelitsas, D. Charistos, A. Tsipis, C. Tsipis, A. Filippidis, C. Triantafyllidis, G. Manos, D. Siapkas, Chem. Eur. J. 17 (2001) 3705.
[53] C. de las Pozas, R. Lopez-Cordero, C. Diaz-Aguila, M. Cora, R. Roque-Malherbe, J. Solid State Chem. 114 (1995) 108.
[54] B. Zibrowius, U. Lohse, J. Richter-Mendau, J. Chem. Soc., Faraday Trans. 87 (1991) 1433.
[55] H. Choo, A.M. Prakash, S.-K. Park, L. Kevan, J. Phys. Chem. B 103 (1999) 6193.
[56] H. Choo, L. Kevan, J. Phys. Chem. B 105 (2001) 6353.
[57] A. Godelitsas, P. Misaelides, D. Charistos, E. Pavlidou, in: P. Misaelides (Ed.), Application of Particle and Laser Beams in Materials Technology, Kluwer Academic Publishers, Dordrecht, 1995, p. 493.
[58] P. Misaelides, A. Godelitsas, S. Kossionidis, G. Manos, Nucl. Instr. and Meth. B 113 (1996) 296.
[59] A. Godelitsas, D. Charistos, J. Dwyer, C. Tsipis, A. Filippidis, A. Hatzidimitriou, E. Pavlidou, Micropor. Mesopor. Mater. 33 (1999) 77.
[60] C. Mosser, A. Mosser, M. Romeo, S. Petit, A. Decarreau, Clays Clay Mineral. 40/5 (1992) 593.
[61] A.H. Al-Saffar, ESR of transition metal ions in zeolites, Ph.D. Thesis, UMIST, UK, 1982.
[62] A. von Zelewsky, J.M. Bemgten, Inorg. Chem. 21 (1982) 1771.
[63] R.J. Blint, J. Phys. Chem. B 100 (1996) 19518.
[64] D. Zhao, R. Szostak, L. Kevan, J. Phys. Chem. B 101 (1997) 5382.

[65] H. Choo, A.M. Prakash, Z. Zhu, L. Kevan, J. Phys. Chem. B 104 (2000) 3608.
[66] H. Choo, S.B. Hong, L. Kevan, J. Phys. Chem. B 105 (2001) 7730.
[67] P. Misaelides, A. Godelitsas, D. Haristos, F. Noli, A. Filippidis, K. Sikalidis, Geol. Carpath. -Ser. CLAYS 44/2 (1993) 115.
[68] P. Misaelides, A. Godelitsas, Toxicol. Environ. Chem. 51 (1995) 21.
[69] R.F.C. Vochten, L. van Haverbeke, F. Goovaerts, J. Chem. Soc. Faraday Trans. 86 (1990) 4095.
[70] A. Godelitsas, P. Misaelides, A. Filippidis, D. Charistos, I. Anousis, J. Radioanal. Nucl. Chem. Articl. 208 (1996) 393.
[71] A. Godelitsas, P. Misaelides, D. Charistos, A. Filippidis, I. Anousis, Chem. Erde 56 (1996) 143.
[72] P. Benard, D. Louer, N. Dacheux, V. Brandel, M. Genet, Chem. Mater. 6 (1994) 1049.
[73] S. Baumann, M.D. Strathman, S.L. Suib, J. Chem. Soc. Chem. Commun. (1986) 308.
[74] P. Wersin, M.F. Hochella Jr., P. Persson, G. Redden, J.O. Leckie, D.W. Harris, Geochim. Cosmochim. Acta 58/13 (1994) 2829.
[75] P. Misaelides, A. Godelitsas, F. Noli, M. Kokkoris, S. Harissopoulos, in: P.A. Sterne, A. Gonis, A.A. Borovoi (Eds.), Actinides and the Environment, Kluwer Academic Publishers, Dordrecht, 1998, p. 303.
[76] P. Misaelides, A. Godelitsas, S. Harissopoulos, I. Anousis, J. Radioanal. Nucl. Chem. 247 (2001) 325.
[77] P. Misaelides, A. Godelitsas, F. Link, H. Baumann, Micropor. Mater. 6 (1996) 37.
[78] P. Misaelides, A. Godelitsas, in: C. Colella, F.A. Mumpton (Eds.), Natural Zeolites for the Third Millenium, De Frede-Editore, Naples, 2000, pp. 229–247.
[79] P.K. Sinha, R.V. Amalraj, V. Krishnasamy, Radiochim. Acta 65 (1994) 125.
[80] J. Kraczka, D.S. Kulgawczuk, A.Z. Hryenkiewicz, Hyperfine Inter. 29 (1986) 1129.
[81] D. Bonnin, G. Calas, Bull. Mineral. 101 (1978) 395.
[82] I. Czako-Nagy, A. Vertes, E. Czaran, J. Papp, J. Radioanal. Nucl. Chem. Lett. 128/1 (1988) 9.
[83] R. Roque-Malherbe, C. Diaz-Aguila, E. Reguera-Ruiz, J. Fundora-Literas, L. Lopez-Colado, M. Hernandez-Velez, Zeolites 10 (1990) 685.
[84] J.F. Marco, M. Gracia, J.R. Gancedo, T. Gonzalez-Carreno, A. Arcoya, X.L. Seoane, Hyperfine Inter. 95 (1995) 53.
[85] P. Misaelides, A. Godelitsas, in: P. Misaelides, F. Macasek, T. Pinnavaia, C. Collela (Eds.), Natural Microporous Materials in Environmental Technology, Kluwer Academic Publishers, Dordrecht, 1999, p. 193.
[86] P. Lukac, N. Patzeltova, M. Foldesova, J. Radioanal. Nucl. Chem. 242 (1999) 231.
[87] M.C. Duff, D.B. Hunter, I.R. Triay, P.M. Bertsch, D.T. Reed, S.R. Sutton, g. Shea-McCarthy, J. Kitten, P. Eng, S.J. Chipera, D.T. Vaniman, Environ. Sci. Technol. 33 (1999) 2163.